Evolution of Resistive Switching Characteristics in WO$_{3-x}$-based MIM Devices by Tailoring Oxygen Deficiency

Krishna Rudrapal[a], Biswajit Jana[b], Venimadhav Adyam[c] and Ayan Roy Chaudhuri[a,b]*

[a]Advanced Technology Development Centre, Indian Institute of Technology Kharagpur, 721302, West Bengal, India

[b]Materials Science Centre, Indian Institute of Technology Kharagpur, 721302, West Bengal, India

[c]Cryogenic Engineering Centre, Indian Institute of Technology Kharagpur, 721302, West Bengal, India

ABSTRACT

We report on resistive switching (RS) characteristics of W/WO$_{3-x}$/Pt-based thin film memristors modulated by precisely controlled oxygen non-stoichiometry. RS properties of the devices with varied oxygen vacancy (V$_O$) concentration have been studied by measuring their DC current voltage properties. Switchability of the resistance states in the memristors have been found to depend strongly on the V$_{OS}$ concentration in the WO$_{3-x}$ layer. Depending on x, the memristors exhibited forming-free bipolar, forming-required bipolar and non-formable characteristics. Devices with high V$_{OS}$ concentration ($\sim 1 \times 10^{21}$ cm^{-3}) exhibited lower initial resistance and memory window of only 15, which has been increased to $\sim$6500 with reducing V$_{OS}$ concentration to $\sim 5.8 \times 10^{20}$ cm^{-3}. Forming-free, stable RS with memory window of $\sim$2000 have been realized for a memristor possessing V$_{OS}$ concentration of $\sim 6.2 \times 10^{20}$ cm^{-3}. Investigation of the conduction mechanism suggests that tailoring V$_{OS}$ concentration modifies the formation and dimension of the conducting filaments as well as the Schottky barrier height at WO$_{3-x}$/Pt interface which deterministically modulates RS characteristics of the WO$_{3-x}$ based memristors.

 INTRODUCTION

Resistive random access memory (RRAM), that stores data in the form of its resistance states defined by the history of applied voltage, has drawn significant research attention for next generation high dense non-volatile memory applications.[1] RRAMs which consist of simple metal-insulator-metal (MIM) structures offer various advantages, such as low power consumption, multiscale switching, scalability, fast operation speed and superior cycling endurance in comparison to the present day charge-based memory technologies. While resistive switching (RS) phenomenon has been reported in diverse class of materials, metal

oxide-based RRAMs that involve modulation of resistance states due to change in the metal valence state (VCM) has drawn significant attention.[2], [3]

Various metal-oxides encompassing binary transition metal oxides (TMOs) such as Ta_2O_5, TiO_2, WO_{3-x}, ZrO_2, NiO, etc., and perovskites e.g. $Pr_{0.7}Ca_{0.3}MnO_3$, $SrTiO_3$, $SrZrO_3$, $BiFeO_3$ etc. have been investigated for their promising VCM type RS.[4]–[10] VCM type RS in metal-oxides often involves formation and rupture of conducting filaments (CFs) due to migration of oxygen vacancies (V_{OS}) under an applied electric field, their generation and annihilation at an active metal-oxide/electrode interface.[11] From the materials point of view, binary TMOs have been widely studied, which are attractive due to their simple structure, low cost, ease of processing, complementary metal–oxide–semiconductor (CMOS) technology compatibility, and promising performance.

Controlling the oxygen non-stoichiometry in binary TMOs through various approaches, such as formation of bilayer structures, utilization of different thin film growth techniques, modification of thin film growth conditions, incorporation of dopants, etc. have been found to play crucial roles in governing their RS properties. Sharath *et al.* demonstrated strong reduction of forming voltage in sub-stoichiometric Ta_2O_{5-x}/TaO_x bilayer thin films with increasing V_{OS} concentration in the TaO_x layer grown under controlled oxygen atmosphere.[12] While bipolar RS had been observed for samples with higher V_{OS} content, the switching transformed to threshold type for samples fabricated at the highest oxidation condition. Yong *et al.* compared the impact of different thin film growth techniques on V_{OS} concentration in HfO_x layers, which influences their forming voltage, memory window (R_{off}/R_{on}) and the Schottky barrier height (SBH) at HfO_x/TiN interface.[13] Skaja *et al.* reported manifestation of reduced forming voltage and high R_{off}/R_{on} upon increasing V_{OS} content in sputter deposited Ta_2O_{5-x} thin films in which V_{OS} concentration had been controlled by sputter power and O_2/Ar ratio.[14] Palhares *et al.* reported on Zr doping in TaO_x thin films as an efficient method of reducing V_{OS} formation

energy, increasing confinement of the CFs which led to reduced device to device variability.[15] Ghenzi *et al.* demonstrated that small variation of O_2/Ar ratio during reactive sputter growth of TiO_{2-x}-based devices led to different RS characteristics, e.g. standard bipolar, electroforming free bipolar and non-switchable device within the same materials system owing to significant variation of V_{OS} concentration.[5] Rehman *et al.* reported tuning of RS characteristics in Zn-doped CeO_2, where concentration and mobility of V_{OS} in CeO_2 has been tuned by Zn dopant concentration.[16] Tunable digital to analogue RS in Nb_2O_5 thin films by V_O engineering has been demonstrated by Xu *et al.*[17] Bousoulas *et al.* discussed that concentration and distribution of V_{OS} in TiO_{2-x} directly influence diameter of the CFs that impacts sensitivity of the conducting paths.[18]

Out of various binary TMOs which exhibit stable RS, WO_3, which is a n-type wide band gap TMO, has been a convenient choice for RS based device applications due to its compatibility with back-end-of-line processing in CMOS integrated circuits.[19] RS properties of WO_3 has been reported to be susceptible to oxygen non-stoichiometry in the oxide layer. Won *et al.* and Rudrapal *et al.* discussed the impact of V_{OS} accumulation on the WO_{3-x}/electrode interface on determining its RS properties.[20], [21] Kim *et al.* reported the role of electrodes with different electronegativities in tuning RS characteristics of WO_3 layers by means of an interfacial suboxide layer formation.[22] Biju *et al.* discussed inhomogeneous distribution of V_{OS} driven changeover of RS mechanism with changing thickness in thermally grown WO_{3-x} films.[23] Yang *et al.* demonstrated on-demand realization of electrical and neuromorphic multifunction in WO_{3-x}-based nanoionic device through externally induced local migration of oxygen ions.[24] Rudrapal *et al.* demonstrated manifestation of forming-free (FF), self-compliant, multi-level RS in WO_{3-x} layers, which has been attributed to reversible oxygen migration at WO_{3-x}/Pt interface.[25], [26] The existing literature reports suggest that, defect engineering based on tuning V_{OS} concentration and assembly in WO_{3-x} thin films holds the potential of

deterministically control their RS properties. However, to the best of our knowledge report on the evolution of RS properties in WO_{3-x} thin films with precise variation of V_{OS} concentration is not present in the literature.

Here, we investigated precisely oxygen tailored WO_{3-x} thin films and correlated variation of their RS characteristics with oxygen content in the layers. On the basis of V_{OS} concentration modulation in WO_{3-x}, we highlighted an effective way to control operating parameters such as forming requirement, set voltage (V_{set}), and R_{off}/R_{on} in $W/WO_{3-x}/Pt$ asymmetric MIM devices and discussed the corresponding switching mechanism. This study enables development of fabrication strategies based on V_{OS} tailoring for realizing CMOS compatible WO_{3-x} based forming free bipolar RS memory devices with a high R_{off}/R_{on} ratio.

RESULTS AND DISCUSSION

All the WO_{3-x} films deposited at room temperature are amorphous in nature which has been confirmed from grazing incidence X-ray difraction (GIXRD) measurements (Figure S1). The samples under investigation possess similar thickness (~42-47 nm), low roughness (<1 nm) and sharp interfaces with the electrodes without the formation of any interfacial layers (Figures S2 and S3).

Figure 1 compares high-resolution X-ray photoelecron spectrocopy (XPS) data around the W 4f and O 1s region for S75, S80, and S85. The binding energies of 35.3 eV and 37.5 eV corresponding to W^{6+} $4f_{7/2}$ and W^{6+} $4f_{5/2}$ respectively.[27] Additionally, two minor peaks appeared at 34.3 eV and 36.5 eV corresponding to the W^{5+} $4f_{7/2}$ and W^{5+} $4f_{5/2}$ respectively. The $4f_{5/2}$ and $4f_{7/2}$ peaks are separated by an expected spin-orbit splitting of 2.2 eV and an area ratio
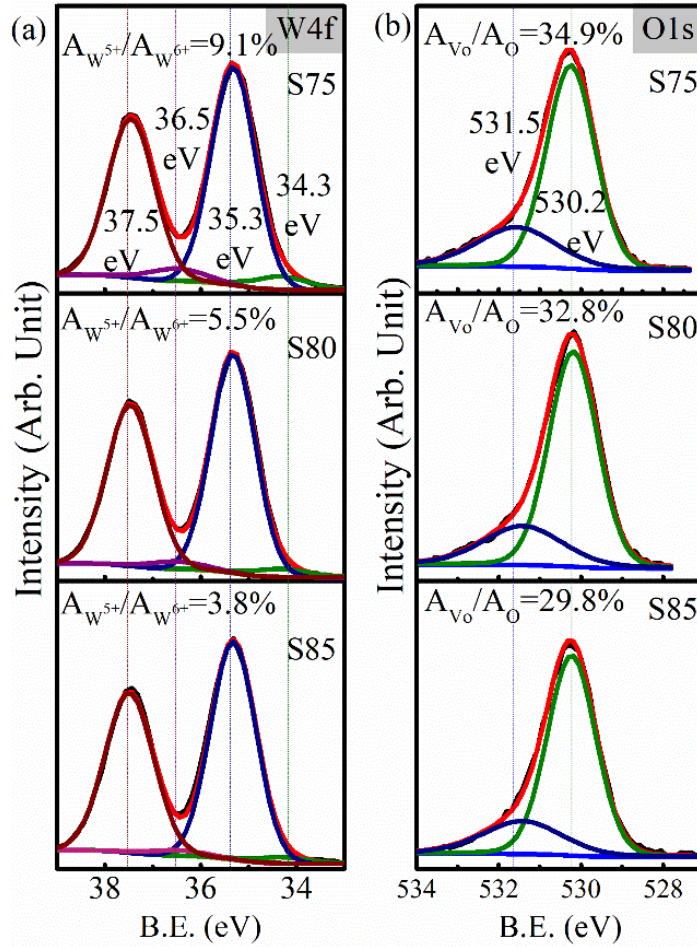
Figure 1. High resolution XPS spectra from sample S75, S80, and S85 with its deconvoluted peak and corresponding area ratio representing variation of stoichiometry with O_2 partial pressure during the growth. (a) W 4f spectra and its corresponding area ratio of W^{5+} to W^{6+} peaks, (b) O 1s and its corresponding area ratio of its non-stoichiometric to lattice oxygen peaks.

of 4:3 for both the oxidation states of W.[20] Manifestation of W^{5+} states in the spectra indicates the formation of non-stoichiometric oxide layers.[27] In case of WO_3, the presence of W^{5+} species is commonly associated with the formation of V_{OS} to maintain charge neutrality.[20], [28] Oxygen non-stoichiometry in the WO_{3-x} layers has also been confirmed from the O 1s peak analysis. The O 1s peak (Figure 1b) could be deconvoluted into two sub-peaks at 530.2 eV and 531.5 eV respectively. While the peak at 530.2 eV represents the oxygen at lattice positions of the stoichiometric oxide layer, the higher energy peak at 531.5 eV represents O atoms in the oxygen-deficient regions of the WO_{3-x} matrix.[25] The degree of
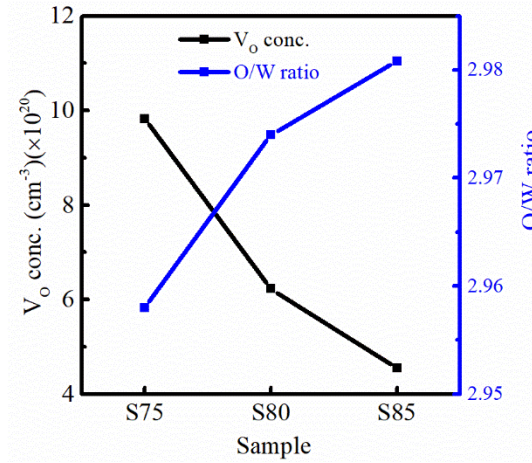
Figure 2. Calculated V_O concentration and O/W ratio for samples S75, S80, and S85. Lines are to guide the eyes. Decrease of V_O and increase of O/W ratio from S75 to S85 is clearly evident.

oxygen non-stoichiometry in the WO_{3-x} layers can be correlated to the area ratio of the O 1s peaks corresponding to the oxygen deficiency and stoichiometric oxygen (A_{Vo}/A_O). The A_{Vo}/A_O ratio has been found to reduce monotonically from 34.9% for S75 to 29.8% for S85. This indicates improvement of oxygen stoichiometry in the sputter-grown WO_{3-x} layers with increasing O_2 partial pressure during deposition. The amount of V_Os in the WO_{3-x} layer has been estimated from the W^{5+}:W^{6+} area ratio (A_W^{5+}/A_W^{6+}).[21] The A_W^{5+}/A_W^{6+} has been found to reduce from 9.1% for S75 to 3.8% for S85. This corresponds to a monotonous reduction of V_Os concentration in the WO_{3-x} layers from 1×10^{21} cm^{-3} (S75) to 4.5×10^{20} cm^{-3} (S85) (Figure 2), representing a change of O/W ratio from ~2.95-2.98. A similar trend of oxygen partial pressure-dependent evolution of V_Os content in DC reactive sputter growth metal oxide thin films has been discussed by Skaja *et al.* for Ta_2O_{5-x} and Ghenzi *et al.* for TiO_{2-x}.[5], [14]

RS characteristics of the non-stoichiometric WO_{3-x} layer have been investigated using W/WO_{3-x}/Pt asymmetric MIM structure. The WO_{3-x} layer possesses sharp interfaces with both top and bottom electrodes as evidenced from cross sectional transmission electron microscopy (TEM) image of a representative sample presented in Figure S3. The inset of Figure 3a represents a schematic of the device structure where DC bias has been applied to the top W electrode and the bottom Pt electrode has been kept grounded. Prior to the RS measurements,

initial resistance (R_i) of the as-fabricated devices has been measured at 0.1 V. Figure 3a represents R_i of all the samples including the device-to-device variability measured over 15 devices from each of the samples. The median value of R_i has been found to monotonically increase from 13 MΩ for S75 to 32 GΩ for S85. Such large variation of intrinsic resistance level by more than three orders of magnitude has been ascribed to difference in concentration of V_{OS} in the WO_{3-x} layers. Lowering of their resistance with increasing V_{OS} is related to the increase in free electron concentration, as V_{OS} act as donors in WO_3.[29] Considering that V_{OS} in WO_{3-x} predominantly manifest as V_O^{2+}, excess electron concentration in the layers due to V_O formation varies between ~2×10^{21} cm^{-3} (S75) to ~9×10^{20} cm^{-3} (S85).[29] The increase in n-type characteristics of the WO_{3-x} layers with increasing V_{OS} concentration has also been confirmed from the reduced separation of Fermi level from the conduction band edge (~1.3 eV for S85 to ~0.7 eV for S75) estimated from investigation of XPS valence band spectra and absorbance spectra from UV-Vis diffuse reflectance spectroscopy (DRS) measurements (Figures S4 and S5).

Figure 3b-f represents room temperature I-V characteristics of the samples under DC voltage sweeps of more than 100 cycles measured in the sequence of 0.0 V→-3.0 V→0.0 V→+3.0 V→0.0 V with a step of 0.05 V and a compliance current set at 1 mA. The compliance current and voltage range used during DC sweep measurements are known to influence on the RS characteristics of the MIM devices significantly.[30] Therefore, the RS characteristics of the samples S75-S83 under investigation have been compared using a constant compliance current (1 mA) and DC bias range (± 3V). Initially, all the as prepared devices have been at high resistance state (HRS) and all, but S85 turned into low resistance state (LRS) when a suitable voltage with negative polarity (V_{set}) has been applied on the top W electrodes initiating the set process. The samples have been reset back to HRS on application of a positive DC bias, representing a bipolar clockwise switching (CWS). Interestingly, the samples S75-S80 having

V_{OS} concentration in the range of $\sim 1 \times 10^{21}$ cm^{-3} - 6.2×10^{20} cm^{-3} exhibited stable bipolar switching without the requirement of any additional electroforming step. This FF nature could be attributed to the large V_{OS} concentration in the WO$_{3-x}$ layers. FF bipolar RS in non-stoichiometric WO$_{3-x}$ having similar V_{OS} density has been reported earlier.[25] However, the sample S83 required an additional forming step that involves application of a larger negative DC bias ($\sim$-4.15 V) prior to exhibiting RS (Figure 3e). Thus, S83 which possesses a lower concentration of V_{OS} ($\sim 5.8 \times 10^{20}$ cm^{-3}) has been termed as a forming-required (FR) device. Further reduction of V_{OS} concentration to $\sim 4.5 \times 10^{20}$ cm^{-3} (S85) rendered the layer to be highly insulating, which could not be switched to LRS even after applying a DC voltage as high as -10 V (inset of Figure 3f), indicating a non-formable (NF) device. This has been attributed to insufficient V_{OS} density in the WO$_{3-x}$ layer which hinders the formation of CFs in the oxide layer.[5] Variation of the I-V characteristics in the WO$_{3-x}$ samples with controlled non-stoichiometry clearly exhibits the deterministic role of V_{OS} on their bipolar RS properties, which change from FF to FR to finally NF device depending on the V_{OS} concentration. V_{OS} concentration-dependent modulation of RS characteristics has been reported earlier in literature for various metal oxides. Sharath *et al.* reported V_{OS} concentration-dependent modulation from FR to FF RS characteristics in HfO$_{2-x}$ thin films.[31] Skaja *et al.* reported a reduction of forming voltage in the case of Ta$_2$O$_{5-x}$ with the increase of V_{OS} concentration.[14] Ghenzi *et al.* observed NF device when the oxygen partial pressure during the TiO$_{2-x}$ layer growth has been increased beyond a certain limit.[5]

In the present study, the nature of RS in all the WO_{3-x} samples under investigation has been associated with gradual change in current with DC voltage sweep. In this case, the V_{set} has been
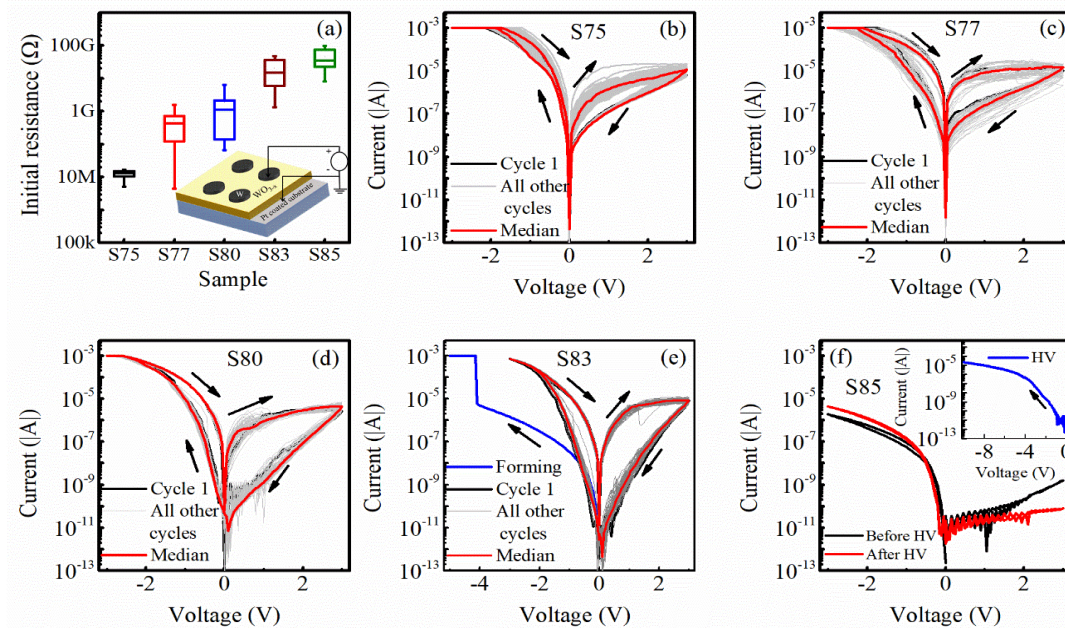

Figure 3. (a) Initial resistance from all the samples taken from 15 devices for each case, inset shows the schematic of the $W/WO_{3-x}/Pt$ device structure with its electrical connections. DC sweep characteristics of the samples with more than 100 sweep cycles (b) S75, (c) S77, (d) S80, (e) S83. (f) DC sweep cycles before and after an application of HV step shows the S85 is a non-switchable device, inset shows the applied HV step. The figure represents evolution of RS with varying V_O-concentrated sample.

defined to be the applied voltage at which current reaches the compliance value, or the maximum applied voltage (-3V) in case current remains below the compliance limit. V_{set} determined for the samples S75-S83 based on this convention has been plotted in Figure 4a. The median value of V_{set} has been found to increase from -1.9 V to -3 V for samples S75 to S83 respectively. Monotonic increase of V_{set} from S75 to S83 is related to the reduced concentration of V_{OS} in the WO_{3-x} layer. Park *et al.* reported an increased V_{set} when the V_{OS} concentration has been reduced by increasing the O_2 flow during the growth of TiO_x layer.[32] It is to be noted that for all the samples the reset voltage (V_{reset}) has been fixed at 3 V.

Figure 4b displays R_{off}/R_{on} of the WO_{3-x} samples determined from the median switching cycles at a read voltage (V_{read}) of +0.5 V. R_{off}/R_{on} increased significantly from ~15 for S75 to ~6500 for S83 indicating an inverse relation with the V_{OS} concertation in the switching layer.
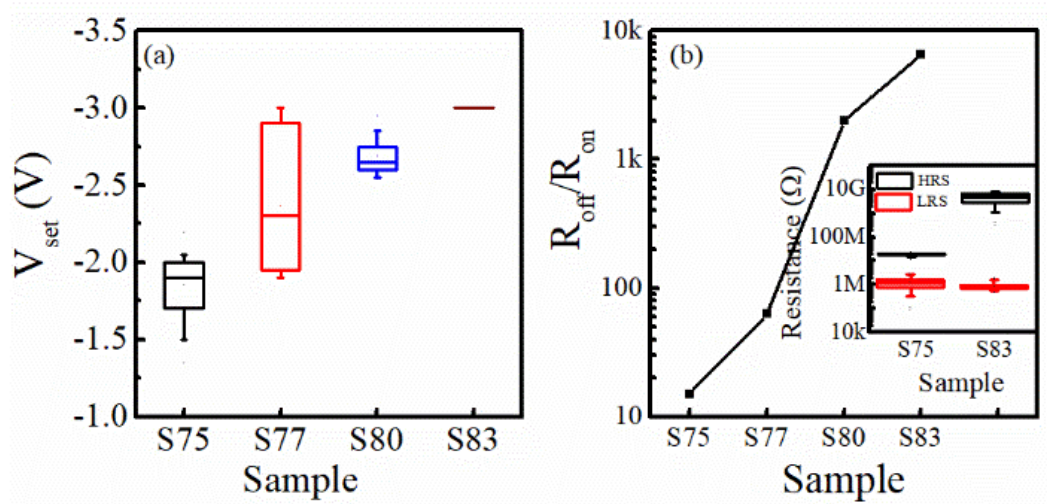

Figure 4. Variation of RS parameters among the samples (a) distribution of V_{set} for each switched sample, it increased from S75 to S83. (b) Extracted R_{off}/R_{on} ratio, it increased almost exponentially from S75 to S83, lines are to guide the eyes, the inset shows the variation of HRS and LRS of S75 and S83.

In order to elucidate the observed trend of R_{off}/R_{on} further, LRS and HRS resistance values (at +0.5 V) of the end members (S75 and S83) of the set of samples considered in this study, has been plotted for 100 cycles and 5 devices (inset of Figure 4b). While the LRS varied marginally around 1 MΩ, the HRS increased significantly (more than three orders of magnitude) from S75 to S83. Clearly, higher HRS resistance in samples with lower V_{OS} concentration leads to the enhanced R_{off}/R_{on}. This has been be attributed to the inferior insulating characteristic of the V_O rich samples and reduced oxygen available to rupture the filament.[31], [33]

SWITCHING MECHANISM

The switching mechanism has been elucidated by investigating the conduction mechanism before and after the switching event. For that, the temperature-dependent DC sweeps were taken for samples from S75 to S83 and the corresponding LRS and HRS data have been plotted

against temperature as shown in Figure 5a and b respectively. For all the WO_{3-x} samples under investigation exhibiting RS, resistance at LRS has been found to increase with increasing temperature, whereas in HRS an opposite trend has been observed. This indicates formation of metallic filaments during the set operation which predominantly control the LRS current, whereas rapture of filaments during the reset step forms the HRS in which the current is controlled by the WO_{3-x}/Pt Schottky junction.[25]
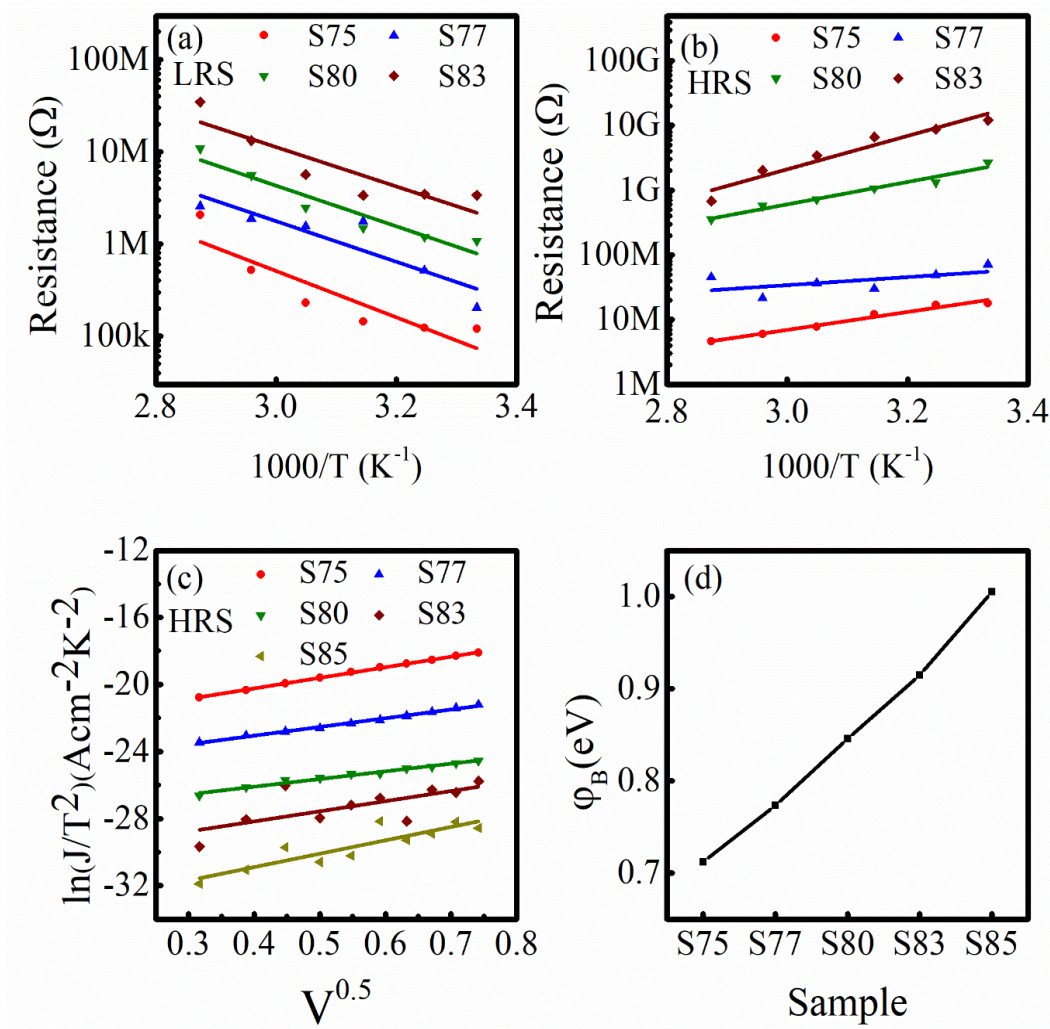

Figure 5. Investigation of the conduction mechanism in the LRS and HRS state. Change of resistances with temperature for all the switchable samples at (a) LRS, indicating metallic-like behavior. (b) HRS, indicating Schottky-like behavior. (c) Fitting of the HRS data for the Schottky emission. (d) Extracted φ_B from each of the sample which shows a monotonic increment from S75 to S85, lines are to aid the eyes.

In order to investigate possible dependence of the Schottky barrier at WO_{3-x}/Pt junction on V_Os concentration in the oxide layer, current conduction in the HRS has been analyzed under the framework Schottky emission theory: [34]

$$J = A * T^2 e^{-\frac{q\left(\varphi_B - \sqrt{\frac{qV}{4\pi\varepsilon_r\varepsilon_0 d}}\right)}{k_B T}} \qquad (1)$$

Where J is current density, A is the effective Richardson constant, T is absolute temperature, q is the electronic charge, φ_B is SBH, V is voltage, $\varepsilon_r, \varepsilon_0$ are the relative and absolute permittivity respectively, d is the space charge width, k_B is the Boltzmann constant.

Figure 5c represents the Richardson's plot [$\ln(J/T^2)$ vs $V^{0.5}$] for the Schottky conduction at HRS. The linear relationship of $\ln(J/T^2)$ vs $V^{0.5}$ is consistent with the Schottky conduction mechanism. Figure 5d demonstrates evolution of SBH (φ_B) at the WO_{3-x}/Pt interface with changing V_Os concentration in the sub-stoichiometric WO_{3-x} layers. φ_B has been found to decrease from 1 eV for S85 to 0.71 for S75, which is consistent with the reduction of SBH with increasing V_Os in metal oxide thin films.[35]–[38]

Next, microscopic mechanism of RS phenomenon in the asymmetric devices with WO_{3-x} layers of varying stoichiometry has been elucidated considering metallic filament-driven LRS and Schottky barrier-driven HRS current. Figure 6 presents a schematic of the proposed RS mechanism in the WO_{3-x} layers considering the S75 and S83 as representative V_Os rich and V_O poor samples respectively. It has been postulated that the V_O concentration is higher at the WO_{3-x}/Pt interface compared to the other parts of the layer. Such a postulation is valid considering that Pt is permeable to oxygen which allows reversible migration and storage of oxygen species in the grain boundaries of Pt in contact with metal oxides.[39]–[41] RS in the present samples involves V_O diffusion due to the concentration gradient, their drift in response to the applied potential and oxygen transfer reaction at the interface with the inert Pt electrode.[25] When a negative bias is applied on the top W electrode, conductive filament

consisting of relatively large density of V_{OS} starts to grow from the cathode toward the anode due to the drift and diffusion flux of V_{OS}. Additionally, V_{OS} gets generated by anodic oxidation at the WO_{3-x}/Pt interface:[35]

$$V_O^{\bullet\bullet}(Pt) + O_O^{\times}(WO_{3-x}) \rightarrow O_O^{\times}(Pt) + V_O^{\bullet\bullet}(WO_{3-x}) \qquad (2)$$
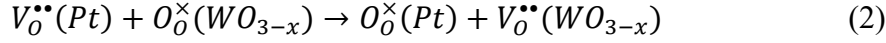
A gradual increase of current with applied bias in all the W/WO_{3-x}/Pt devices under investigation (Figure 3) suggests a competition between V_O drift and diffusion migration towards W cathode, and oxygen exchange reaction at the high-work function Pt electrode. Considering a much lower diffusion coefficient of oxygen in Pt compared to WO_3, certain depletion of V_{OS} in WO_{3-x} near its interface with Pt can take place.[42], [43] In such case, V_{OS}
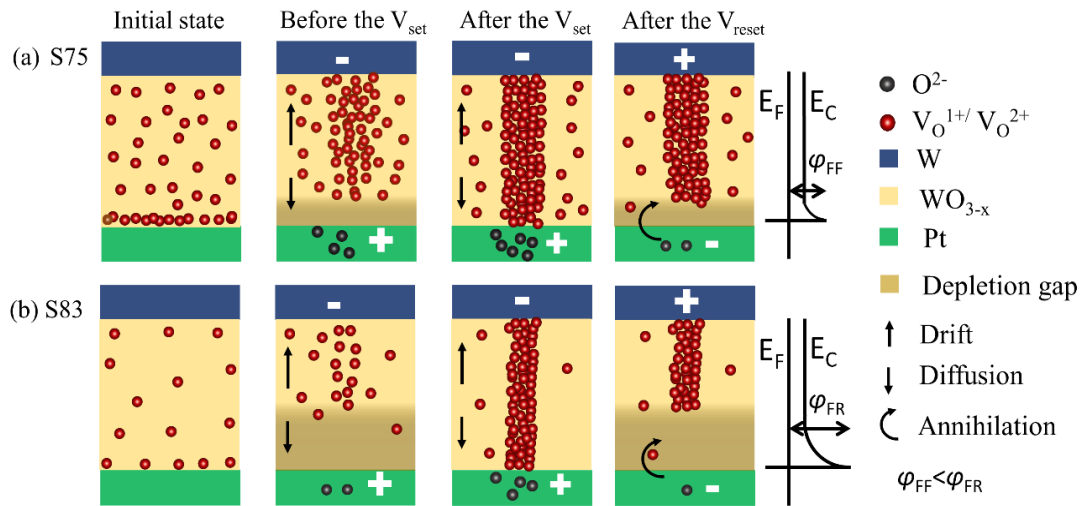

Figure 6. Schematic representation of the proposed switching mechanism through the initial, set, and reset process along with the evolution of filament and depletion gap depending on the V_{OS} concentration for (a) S75, (b) S83.

migration towards cathode shall dominate over the oxygen extraction at anode, giving rise to a high insulating region near the WO_{3-x}/Pt interface. Formation of a V_O depleted region near the anode induces a reverse concentration gradient (from cathode to anode) which eventually drives V_{OS} diffusion towards the anode and reduces the depletion gap. At an adequately large applied voltage, the V_{OS} generation flux at the anode also increases which aids to the filament formation. Finally at the V_{set}, the formation of the conductive filament gets completed when LRS sets in. The observed difference in V_{set} for all the samples under consideration has been

attributed to their initial V_{OS} concentration and V_{OS} generation at the WO_{3-x}/Pt interface. As evident from Figure 3a, electrical conductivity (σ) of the WO_{3-x} layers increases with increase in V_{OS} concentration in the layer. Considering V_{OS} formation barrier at a metal-oxide/anode interface to be a constant, the V_{OS} depletion gap varies inversely with σ of the oxide layer.[44] Therefore, it is postulated that V_{OS} depletion gap at the WO_{3-x}/Pt interface increases from S75 to S85 in accordance to their increasing electrical resistances. Since V_{OS} generation rate at the oxide/anode interface gets prompted by the heat generation due to Joule heating effect, V_{set} reduces from S83 (having lower σ) to S75 (having higher σ). This is further established by the fact that while WO_{3-x} samples S75-S80 ($[V_O] \sim 1 \times 10^{21}$ cm^{-3}-6.2×10^{20} cm^{-3}) exhibit forming free RS, a forming step is required for the sample S83 ($[V_O] \sim 5.8 \times 10^{20}$ cm^{-3}) and S85 ($[V_O] \sim 4.5 \times 10^{20}$ cm^{-3}) did not exhibit any RS at all even after applying a voltage as high as -10 V.

In order to further elucidate the influence of CFs on the conduction behaviour of WO_{3-x} layers, resistance states of S75 and S83 have been compared at -0.5V (Figure S6). While resistance of the LRS increased by 10 times from S75 to S83, the HRS increased by 1000 times. Under the framework of filamentary conduction model, increase LRS resistance with decreasing V_{OS} suggests a higher filament resistance. This is attributed to the reduction of filament diameter with reducing V_{OS} concentration from S75 to S83. Reduction of CFs' diameter with reducing V_{OS} concentration in metal-oxide layers has been reported for TiO_{2-x} and NbO_x based RS devices.[5], [18], [45] Such difference in the LRS resistance has not been observed when measured at +0.5V during reset cycles (Figure 4b). During the reset operation for bipolar RS observed in the present study, when a positive bias is applied on the W top electrode, V_{OS} annihilation at the WO_{3-x}/Pt takes place:

$$O_O^\times(Pt) + V_O^{\bullet\bullet}(WO_{3-x}) \rightarrow V_O^{\bullet\bullet}(Pt) + O_O^\times(WO_{3-x}) \qquad (3)$$
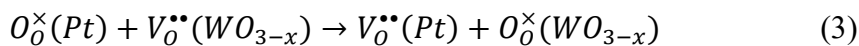
As a result, partial dissolution of filament starts to re-establish the Schottky junction, and current conduction during the reset cycle begins to get controlled also by the Schottky barrier

at the WO_{3-x}/Pt interface even before complete reset. The nature of the V_{OS} depleted region and the CF determines the LRS resistance during reset operation. Similarly, large difference of the HRS resistance between S75 and S83 at a read voltage of -0.5V is attributed to the better oxidation of the samples which present a higher barrier to the conduction of electrons prior to the set process.

CONCLUSIONS

In summary, fabrication of amorphous WO_{3-x} thin films by DC reactive sputtering under varying the O_2/Ar ratio provides an effective method of inducing precisely controlled oxygen non-stoichiometry in the oxide layers. XPS investigation confirmed stoichiometry variation which corresponds to V_{OS} concentration ranging between $\sim 4.5 \times 10^{20}$ cm^{-3} to $\sim 1 \times 10^{21}$ cm^{-3} in the WO_{3-x} layers grown under different O_2/Ar ratio. Increase in V_{OS} with reduced O_2/Ar ratio has been found to increase conductivity of the oxide layers which is attributed to the enhanced free electron concentration in the n-type WO_{3-x}. DC I-V measurements on the $W/WO_{3-x}/Pt$ devices provided the evidence that V_{OS} concentration plays a significant role in their RS characteristics. Low concentration of V_{OS} ($\leq 4.5 \times 10^{20}$ cm^{-3}) suppresses the formation of CFs thus rendering the devices non-switchable. Increase in V_{OS} concentration to $\sim 5.8 \times 10^{20}$ cm^{-3} leads to a switchable device after inducing an electroforming step, while the devices with higher V_{OS} concentration ($V_O = 6.2 \times 10^{20}$ cm^{-3} to 1×10^{21} cm^{-3}) exhibit forming free bipolar RS. Further, the set voltage and memory window of the devices have been found to reduce with increasing V_{OS} concentration. Analysis of the DC I-V characteristics establishes that modulation of RS characteristics in the WO_{3-x} layers relates to the CF diameter, their formation and dissolution due to V_{OS} diffusion under concentration gradient, their drift in response to the applied potential and oxygen transfer reaction at the WO_{3-x}/Pt interface. Our work has provided

strong proof that RS characteristics of CMOS compatible are deterministically tunable by V_{OS} engineering.

EXPERIMENTAL DETAILS

The WO_{3-x} layers have been deposited on Pt (~34 nm)/Ti(~5 nm)/SiO_2(~300 nm)/Si(100) substrate. Before any deposition, the substrates have been cleaned by dipping sequentially in Trichloroethylene, Acetone, and Methanol for 5 min for each case in an ultrasonic bath. After that, it has been rinsed with de-ionized (DI) water and dried with a nitrogen blower. The chamber had been evacuated to a base pressure of 7.5×10^{-4} mTorr prior to the oxide layer deposition. The depositions were carried out at room temperature by DC reactive sputtering using a commercial tungsten target (advanced engineering materials, purity >99.99%) with a chamber pressure of 5 mTorr. In order to achieve varied oxygen non-stoichiometry in the WO_{3-x} layers, five samples (Table 1) have been grown with oxygen partial pressure during the growth varying from 75% to 85% in a mixture of oxygen and argon gas (O_2/Ar) keeping all the other parameters unchanged. The samples have been prepared by maintaining a target-to-substrate distance of 10 cm and DC power density of 1.23 Watt/cm^2. MIM structures for investigating RS properties have been prepared by depositing W dots with a diameter of 100 µm on the WO_{3-x} thin films by DC sputtering through a shadow mask.

The structural property has been investigated by GIXRD using X-ray source of CuKα1 having a wavelength of 1.5406 Å (PANalytical, Empyrean). The diffraction patterns were collected with a step size of 0.06° in the 2θ range of 20–60°. The incidence angle of CuKα radiation was kept at 0.4° relative to the sample surface. The X-ray reflectivity (XRR) measurements were done in the same instrument and the fittings were done using the AMaaS software. The device structure was confirmed by a cross-section transmission electron microscope (TEM) (FEI TECNAI G2 F20 X-TWIN) image. Bandgap was measured through

UV-Vis DRS. Chemical analysis and valence band spectra of the oxide layers have been done using XPS (PHI 5000 VersaProbe III, USA) measurements with monochromatic Al Kα X-rays (spot diameter 100 μm). Deconvolution of the XPS spectra includes Shirley-type baseline subtraction and profile fitting through the Lorentzian-Gaussian function. The C1s peak at 284.5 eV has been taken as a reference point for all the binding energy calculations. DC current-voltage (I-V) measurements were carried out by Keithley 4200-SCS keeping a step size of 0.05 V. A JANIS probe station (model no: ST500-UHT-1-(4CX)) has been used to probe the samples.

Table 1. Variation of sputtering deposition parameters for WO_{3-x} films

Sample	O_2 partial pressure
S75	75%
S77	77%
S80	80%
S83	83%
S85	85%

AUTHOR INFORMATION

Corresponding Author

*A. Roy Chaudhuri

Email: ayan@matsc.iitkgp.ac.in

Author Contributions

A.R.C conceived the idea. A.R.C and K.R designed the experiments, executed the measurements and analyzed the data. B.J contributed in the experiments. A.R.C and V.A

supervised the work. All the authors discussed the results and have given approval to the final version of the manuscript.

Notes

Authors declare no competing financial interest.

REFERENCES

[1]   Beyond CMOS, "International Roadmap for Devices and Systems," 2020. [Online]. Available: https://irds.ieee.org.

[2]   I. Valov, "Interfacial interactions and their impact on redox-based resistive switching memories (ReRAMs)," *Semicond. Sci. Technol.*, vol. 32, no. 9, p. 093006, Sep. 2017, doi: 10.1088/1361-6641/aa78cd.

[3]   J. Y. Chen, C. W. Huang, C. H. Chiu, Y. T. Huang, and W. W. Wu, "Switching Kinetic of VCM-Based Memristor: Evolution and Positioning of Nanofilament," *Adv. Mater.*, vol. 27, no. 34, pp. 5028–5033, 2015, doi: 10.1002/adma.201502758.

[4]   W. Y. Chang *et al.*, "Improvement of resistive switching characteristics in TiO_2 thin films with embedded Pt nanocrystals," *Appl. Phys. Lett.*, vol. 95, no. 4, p. 042104, Jul. 2009, doi: 10.1063/1.3193656.

[5]   N. Ghenzi, M. J. Rozenberg, R. Llopis, P. Levy, L. E. Hueso, and P. Stoliar, "Tuning the resistive switching properties of TiO_{2-x} films," *Appl. Phys. Lett.*, vol. 106, no. 12, p. 123509, Mar. 2015, doi: 10.1063/1.4916516.

[6]   V. K. Sahu, P. Misra, R. S. Ajimsha, A. K. Das, M. P. Joshi, and L. M. Kukreja, "Resistive memory switching in ultrathin TiO_2 films grown by atomic layer deposition," in *AIP Conference Proceedings*, 2016, p. 120032, doi: 10.1063/1.4948104.

[7]   M.-J. Lee *et al.*, "A fast, high-endurance and scalable non-volatile memory device made from asymmetric Ta_2O_{5-x}/TaO_{2-x} bilayer structures," *Nat. Mater.*, vol. 10, no. 8, pp. 625–630, 2011, doi: 10.1038/nmat3070.

[8]   A. R. Lee *et al.*, "Multifunctional resistive switching behaviors employing various electroforming steps," *J. Mater. Chem. C*, vol. 4, no. 4, pp. 823–830, 2016, doi: 10.1039/C5TC03303A.

[9]   A. Kawahara *et al.*, "An 8 mb multi-layered cross-point ReRAM macro with 443 MB/s write throughput," *IEEE J. Solid-State Circuits*, vol. 48, no. 1, pp. 178–185, 2013, doi: 10.1109/JSSC.2012.2215121.

[10]   S. Kim *et al.*, "Ultrathin (<10nm) Nb2O5/NbO2 hybrid memory with both memory and selector characteristics for high density 3D vertically stackable RRAM applications," in *2012 Symposium on VLSI Technology (VLSIT)*, Jun. 2012, pp. 155–156, doi: 10.1109/VLSIT.2012.6242508.

[11]   F. Pan, S. Gao, C. Chen, C. Song, and F. Zeng, "Recent progress in resistive random

access memories: Materials, switching mechanisms, and performance," *Mater. Sci. Eng. R Reports*, vol. 83, no. 1, pp. 1–59, 2014, doi: 10.1016/j.mser.2014.06.002.

[12]   S. U. Sharath *et al.*, "Impact of oxygen stoichiometry on electroforming and multiple switching modes in TiN/TaO$_x$/Pt based ReRAM," *Appl. Phys. Lett.*, vol. 109, no. 17, p. 173503, Oct. 2016, doi: 10.1063/1.4965872.

[13]   Z. Yong *et al.*, "Tuning oxygen vacancies and resistive switching properties in ultra-thin HfO$_2$ RRAM via TiN bottom electrode and interface engineering," *Appl. Surf. Sci.*, vol. 551, no. March, p. 149386, 2021, doi: 10.1016/j.apsusc.2021.149386.

[14]   K. Skaja, M. Andrä, V. Rana, R. Waser, R. Dittmann, and C. Baeumer, "Reduction of the forming voltage through tailored oxygen non-stoichiometry in tantalum oxide ReRAM devices," *Sci. Rep.*, vol. 8, no. 1, pp. 1–7, 2018, doi: 10.1038/s41598-018-28992-9.

[15]   J. H. Q. Palhares *et al.*, "Oxygen vacancy engineering of TaO$_x$-based resistive memories by Zr doping for improved variability and synaptic behavior," *Nanotechnology*, vol. 32, no. 40, p. 405202, Oct. 2021, doi: 10.1088/1361-6528/ac0e67.

[16]   S. Rehman, H. Kim, M. Farooq Khan, J. H. Hur, A. D. Lee, and D. kee Kim, "Tuning of ionic mobility to improve the resistive switching behavior of Zn-doped CeO$_2$," *Sci. Rep.*, vol. 9, no. 1, pp. 1–10, 2019, doi: 10.1038/s41598-019-55716-4.

[17]   J. Xu *et al.*, "Tunable digital-to-analog switching in Nb$_2$O$_5$-based resistance switching devices by oxygen vacancy engineering," *Appl. Surf. Sci.*, vol. 579, no. November 2021, p. 152114, 2022, doi: 10.1016/j.apsusc.2021.152114.

[18]   P. Bousoulas, I. Michelakaki, and D. Tsoukalas, "Influence of oxygen content of room temperature TiO$_{2-x}$ deposited films for enhanced resistive switching memory

performance," *J. Appl. Phys.*, vol. 115, no. 3, p. 034516, Jan. 2014, doi: 10.1063/1.4862797.

[19] M. N. Kozicki, C. Gopalan, M. Balakrishnan, and M. Mitkova, "A low-power nonvolatile switching element based on copper-tungsten oxide solid electrolyte," *IEEE Trans. Nanotechnol.*, vol. 5, no. 5, pp. 535–544, 2006, doi: 10.1109/TNANO.2006.880407.

[20] S. Won, S. Y. Lee, J. Park, and H. Seo, "Forming-less and Non-Volatile Resistive Switching in WO_x by Oxygen Vacancy Control at Interfaces," *Sci. Rep.*, vol. 7, no. 1, pp. 1–8, 2017, doi: 10.1038/s41598-017-10851-8.

[21] K. Rudrapal, A. Mukherjee, V. Adyam, and A. Roy Chaudhuri, "Modulation of resistive switching properties of non-stoichiometric WO_{3-x} based asymmetric MIM structure by interface barrier modification," *J. Appl. Phys.*, vol. 129, no. 23, p. 235302, 2021, doi: 10.1063/5.0053511.

[22] J. Kim *et al.*, "Effect of Electronegativity on Bipolar Resistive Switching in a WO_3-Based Asymmetric Capacitor Structure," *ACS Appl. Mater. Interfaces*, vol. 8, no. 14, pp. 9499–9505, 2016, doi: 10.1021/acsami.5b11781.

[23] J. Shin *et al.*, "TiO_2-based metal-insulator-metal selection device for bipolar resistive random access memory cross-point application," *J. Appl. Phys.*, vol. 109, no. 3, pp. 2–5, 2011, doi: 10.1063/1.3544205.

[24] R. Yang *et al.*, "On-demand nanodevice with electrical and neuromorphic multifunction realized by local ion migration," *ACS Nano*, vol. 6, no. 11, pp. 9515–9521, 2012, doi: 10.1021/nn302510e.

[25] K. Rudrapal, G. Bhattacharya, V. Adyam, and A. Roy Chaudhuri, "Forming-Free, Self-

Compliance, Bipolar Multi-Level Resistive Switching in WO_{3-x} Based MIM Device," *Adv. Electron. Mater.*, vol. 2200250, p. 2200250, Jun. 2022, doi: 10.1002/aelm.202200250.

[26] E. Sutter and P. Sutter, "Enhanced oxidation of nanoscale In particles at the interface with a Si nanowire," *Appl. Phys. Lett.*, vol. 100, no. 23, p. 231602, Jun. 2012, doi: 10.1063/1.4726054.

[27] A. H. Y. Hendi *et al.*, "Modulation of the band gap of tungsten oxide thin films through mixing with cadmium telluride towards photovoltaic applications," *Mater. Res. Bull.*, vol. 87, pp. 148–154, 2017, doi: 10.1016/j.materresbull.2016.11.032.

[28] M. B. Johansson, P. T. Kristiansen, L. Duda, G. A. Niklasson, and L. Österlund, "Band gap states in nanocrystalline WO_3 thin films studied by soft x-ray spectroscopy and optical spectrophotometry," *J. Phys. Condens. Matter*, vol. 28, no. 47, p. 475802, Nov. 2016, doi: 10.1088/0953-8984/28/47/475802.

[29] W. Wang, A. Janotti, and C. G. Van De Walle, "Role of oxygen vacancies in crystalline WO_3," *J. materals Chem. C*, vol. 4, pp. 6641–6648, 2016, doi: 10.1039/c6tc01643j.

[30] Y. Li, P. Yuan, L. Fu, R. Li, X. Gao, and C. Tao, "Coexistence of diode-like volatile and multilevel nonvolatile resistive switching in a ZrO_2 /TiO_2 stack structure," *Nanotechnology*, vol. 26, no. 39, p. 391001, Oct. 2015, doi: 10.1088/0957-4484/26/39/391001.

[31] S. U. Sharath *et al.*, "Towards forming-free resistive switching in oxygen engineered HfO_{2-x}," *Appl. Phys. Lett.*, vol. 104, no. 6, p. 063502, 2014, doi: 10.1063/1.4864653.

[32] S.-J. Park *et al.*, "In situ control of oxygen vacancies in TiO_2 by atomic layer deposition for resistive switching devices," *Nanotechnology*, vol. 24, no. 29, p. 295202, Jul. 2013,

doi: 10.1088/0957-4484/24/29/295202.

[33] F. M. Simanjuntak, D. Panda, T. L. Tsai, C. A. Lin, K. H. Wei, and T. Y. Tseng, "Enhancing the memory window of AZO/ZnO/ITO transparent resistive switching devices by modulating the oxygen vacancy concentration of the top electrode," *J. Mater. Sci.*, vol. 50, no. 21, pp. 6961–6969, 2015, doi: 10.1007/s10853-015-9247-y.

[34] S. M. Lim *et al.*, "Thermally Stable Amorphous Oxide-based Schottky Diodes through Oxygen Vacancy Control at Metal/Oxide Interfaces," *Sci. Rep.*, vol. 9, no. 1, pp. 1–9, 2019, doi: 10.1038/s41598-019-44421-x.

[35] D. S. Jeong, H. Schroeder, and R. Waser, "Mechanism for bipolar switching in a $Pt/TiO_2/Pt$ resistive switching cell," *Phys. Rev. B*, vol. 79, no. 19, p. 195317, May 2009, doi: 10.1103/PhysRevB.79.195317.

[36] Y. L. Chung, P. Y. Lai, Y. C. Chen, and J. S. Chen, "Schottky barrier mediated single-polarity resistive switching in Pt layer-included TiO_x memory device," *ACS Appl. Mater. Interfaces*, vol. 3, no. 6, pp. 1918–1924, 2011, doi: 10.1021/am200106z.

[37] M. K. Niranjan and R. Mamindla, "Schottky barrier height and modulation due to interface structure and defects in Pt|MgO|Pt heterojunctions with implications for resistive switching," *J. Appl. Phys.*, vol. 127, no. 20, p. 205306, May 2020, doi: 10.1063/1.5143658.

[38] J. J. Yang, M. D. Pickett, X. Li, D. A. A. Ohlberg, D. R. Stewart, and R. S. Williams, "Memristive switching mechanism for metal/oxide/metal nanodevices," *Nat. Nanotechnol.*, vol. 3, no. 7, pp. 429–433, 2008, doi: 10.1038/nnano.2008.160.

[39] R. Schmiedl *et al.*, "Oxygen diffusion through thin Pt films on Si(100)," *Appl. Phys. A Mater. Sci. Process.*, vol. 62, no. 3, pp. 223–230, Feb. 1996, doi:

10.1007/s003390050289.

[40]   S. Oh *et al.*, "Oxygen activation on the interface between Pt nanoparticles and mesoporous defective TiO_2 during CO oxidation," *J. Chem. Phys.*, vol. 151, no. 23, p. 234716, Dec. 2019, doi: 10.1063/1.5131464.

[41]   D. S. Jeong, H. Schroeder, U. Breuer, and R. Waser, "Characteristic electroforming behavior in $Pt/TiO_2/Pt$ resistive switching cells depending on atmosphere," *J. Appl. Phys.*, vol. 104, no. 12, p. 123716, Dec. 2008, doi: 10.1063/1.3043879.

[42]   V. K. Sikka and C. J. Rosa, "The oxidation kinetics of tungsten and the determination of oxygen diffusion coefficient in tungsten trioxide," *Corros. Sci.*, vol. 20, no. 11–12, pp. 1201–1219, Jan. 1980, doi: 10.1016/0010-938X(80)90092-X.

[43]   L. R. Velho and R. W. Bartlett, "Diffusivity and solubility of oxygen in platinum and Pt-Ni alloys," *Metall. Mater. Trans. B 1972 31*, vol. 3, no. 1, pp. 65–72, Jan. 1972, doi: 10.1007/BF02680586.

[44]   K. Zhang, Y. Ren, P. Ganesh, and Y. Cao, "Effect of electrode and oxide properties on the filament kinetics during electroforming in metal-oxide-based memories," *npj Comput. Mater.*, vol. 8, no. 1, pp. 1–10, 2022, doi: 10.1038/s41524-022-00770-2.

[45]   J. Aziz *et al.*, "Effect of oxygen stoichiometry on the threshold switching of RF-sputtered NbO_x (x = 2.0–2.5) films," *Mater. Res. Bull.*, vol. 144, no. June, p. 111492, Dec. 2021, doi: 10.1016/j.materresbull.2021.111492.